

## **3.4 Cryosphere-related Algorithms**

### 3.4.1 CTSK1

#### A. Algorithm Outline

(1) Algorithm Code: CTSK1

(2) Product Code: CLFLG\_p

(3) PI Name: Dr. Knut Stamnes

#### (4) Overview of Algorithm

This algorithm theoretical basis document (ATBD) describes the algorithm development for the cloudy/clear discriminator (ADEOS-II/GLI/CTSK1a) and the snow/sea-ice discriminator (ADEOS-II/GLI/CTSK1b) to be applied in the polar regions and in snow-covered mid-latitude areas. We present the theoretical basis for the algorithm, processing flow charts, and its application to MODIS Airborne Simulator (MAS) data. The calibrated radiance data at level 1B of GLI measurements in channels 8, 13, 17, 19, 24, 27, 30, 31, 34, 35, and 36 will be used as input to this algorithm. The algorithm is based on pre-defined thresholds. The snow/sea-ice discriminator works only during daytime. Fortunately, bare sea-ice conditions are expected to occur primarily in summer, and the bright polar summer will offer the opportunity to use the snow/sea-ice discriminator. The output of the cloudy/clear and snow/sea-ice discriminator algorithm will be an 8-bit word for each field of view. It includes information about whether a view of the surface is obstructed by cloud and the surface type for each pixel. The output of the algorithm is not a simple yes/no judgment for cloudy/clear discrimination. There are four levels of *confidence* to indicate whether a pixel is judged to be cloudy or clear. In addition, this algorithm also allows for on-screen display of a color image of the output file of a scene remotely-sensed by satellite. This color image will be a plot of the distribution of cloud and various types of surfaces. The output file of this algorithm is also an important and necessary input for cloud and surface property retrieval algorithms as well as other related studies.

## B. Theoretical Description

### (1) Methodology and Logic Flow

#### 1. Input and Output

##### 1.1 Input

As mentioned above, the calibrated radiance data of GLI at level 1B in channels 8, 13, 17, 19, 24, 27, 30, 31, 34, 35, and 36 will be used as input for the algorithm. If there are any incomplete and bad data in these channels for a pixel being remotely-sensed, the first bit (bit 0) of the 8-bit output word (see below) will be set to 0 for this pixel, and then the algorithm will not be executed. Thus a hole will be created in the final output map. Additionally, several ancillary data sets are required as input to the algorithm:

- Sun position and sensor position, i.e., zenith and azimuthal angles for both the sun and the satellite sensor
- The latitudes and longitudes for the current scan area
- A land/water map with 1 km resolution
- GLI surface-identification maps for the previous 8 or 4 days that will be used for the temporal uniformity test

##### 1.2 Output

The output of the cloudy/clear and snow/sea-ice discriminator algorithm will be an 8-bit word for each field of view. The output bit structure is shown in Table 2.1. The output file consists of the results of cloud mask (i.e., cloudy or clear) and the results of surface identification for cloud-free pixels. In some cases, however, it is still ambiguous to define whether a pixel is cloudy or not. For example, a pixel may be partially cloudy, or a pixel may appear cloudy at one spectral channel but appear cloud-free at another channel. A brightness temperature difference test, based on the 10.8 and 3.7  $\mu\text{m}$  channels, is sensitive to water clouds, but not to thin cirrus. In contrast, the 1.38  $\mu\text{m}$  channel is sensitive to the presence of high level cirrus due to the strong water vapor absorption. Thus, multi-spectral approaches are expected to be particularly useful for cloud detection in the polar regions. The output of the algorithm is not a simple yes/no judgment for cloudy/clear discrimination. There are 4 levels of *confidence* to indicate whether a pixel is judged to be cloudy or not (bit 2-1 of the output word) based on the analysis of the results from different spectral tests.

A brief description of the output bits is given as follows (see Table 2.1):

Table 2.1 The output of the cloudy/clear and snow/sea-ice discriminator algorithm. The output is an 8-bit word, i.e.,

7-6	5-3	2-1	0
-----	-----	-----	---

Bit No.	Bit output	Meaning	Remark
bit 0	0	not executed	
	1	executed	
bit 2-1	00	clear sky	
	01	high-confidence cloudy	confidence = 100%
	10	middle-confidence cloudy	50% confidence <100%
	11	low-confidence cloudy	0% < confidence < 50%
bit 5-3	000	snow over ice	
	001	sea ice	
	010	cloud shadow on snow	
	011	land with vegetation	
	100	open ocean	
	101	snow over land	
	110	snow over land contaminated with vegetation	
	111	bare land with less vegetation	
bit 7-6			Spares

- Bit 0: If the sensor-measured radiance of a pixel is deemed to be *bad*, bit 0 will be set to 0, and the algorithm will not be executed for this pixel. If the algorithm is executed normally bit 0 will be set to 1.
- Bit 2-1: Bit 2-1 represents the final results of the cloudy/clear discrimination processing. For a given pixel bit 2-1 indicates clear or cloudy with different confidence levels (see Table 2.1).

Based on the threshold value for each individual cloud test, a confidence flag is assigned. There is a linear interpolation between the high-confidence-cloud threshold (100%) and the clear-sky threshold (0%). If the confidence is 100%, bit 2-1 is set to 01. If the confidence is between 50% and 100%, bit 2-1 is set to 10. If the confidence is between 0% and 50%, bit 2-1 is set to 11. For the case with confidence of 0%, bit 2-1 is set to 00, and the pixel is assumed to be clear (cloud-free).

Because various test techniques (or methods) may be sensitive to different kinds of cloud, the final determination will be made by considering the maximum confidence of all tests applied. This implies that the algorithm will be cloud conservative. For a pixel with low-

confidence cloud, additional spatial and temporal consistency tests will be implemented for improving the cloudy/clear discrimination capability.

- Bit 5-3: For a clear pixel (bit 2-1 is set to 00), the algorithm will assign the surface type. Generally, the thresholds for reflectance and brightness temperature can be used to distinguish pixels with snow/sea-ice from pixels with the land/open-ocean. The land/water map will be used to flag land and ocean. Further, the snow/sea-ice discriminator will be used to distinguish the bare sea-ice from snow-covered sea-ice and/or open water in ocean areas. There are five surface types that will be tagged by this algorithm: snow (including snow-covered sea-ice), bare sea-ice (snow-free), land (including vegetation), open ocean, and cloud shadow over snow. The cloud shadow test will be implemented only over snow during daytime.

In addition, this algorithm can also offer the ability to plot a color image of the processing results. The color image will be a plot of the distribution of cloud and various types of surface. It provides a visualization useful for testing our understanding of the algorithm. The output file of this algorithm is also an important and necessary input for cloud retrieval and surface property retrieval algorithms as well as other related studies.

## 2. Implementation of the Algorithm

The algorithm includes four parts: cloudy/clear discriminator, snow/sea-ice discriminator, cloud shadow detection, and surface classification (as shown in Figure 2.1). It can be used to identify clear scenes and to provide surface classification. Sea-ice will be classified into bare sea-ice and snow-covered sea-ice. This information will be saved in an output file consisting of an 8-bit word for each pixel that is required for retrieval of cloud and surface properties.

The cloudy/clear discriminator consists of a daytime mode and a nighttime mode. In each mode, there are two independent tests for detection of low cloud and thin cirrus cloud. Because surface temperature inversions often exist under clear-sky conditions during polar winter, a temperature inversion test will be included in both the daytime mode and the night time mode to improve the capability of cloud detection. The result of each test is expressed as a *confidence* level that indicates the likelihood that the pixel is contaminated with cloud. The final confidence level is determined by the maximum confidence level resulting from applying several tests. Most pixels have either confidence 1 (high confidence cloud) or 0 (clear pixel). Pixels with an intermediate confidence value, tend to be found at cloud boundaries.

For clear pixels, surface classification will be applied to tag the surface as land, open ocean, snow-covered land, or snow/ice-covered ocean. Each clear pixel will be classified as being

land or ocean according to its location in the land/water map. Simple reflectance and/or brightness temperature threshold tests are used to distinguish snow/ice-covered surface from land or open ocean.

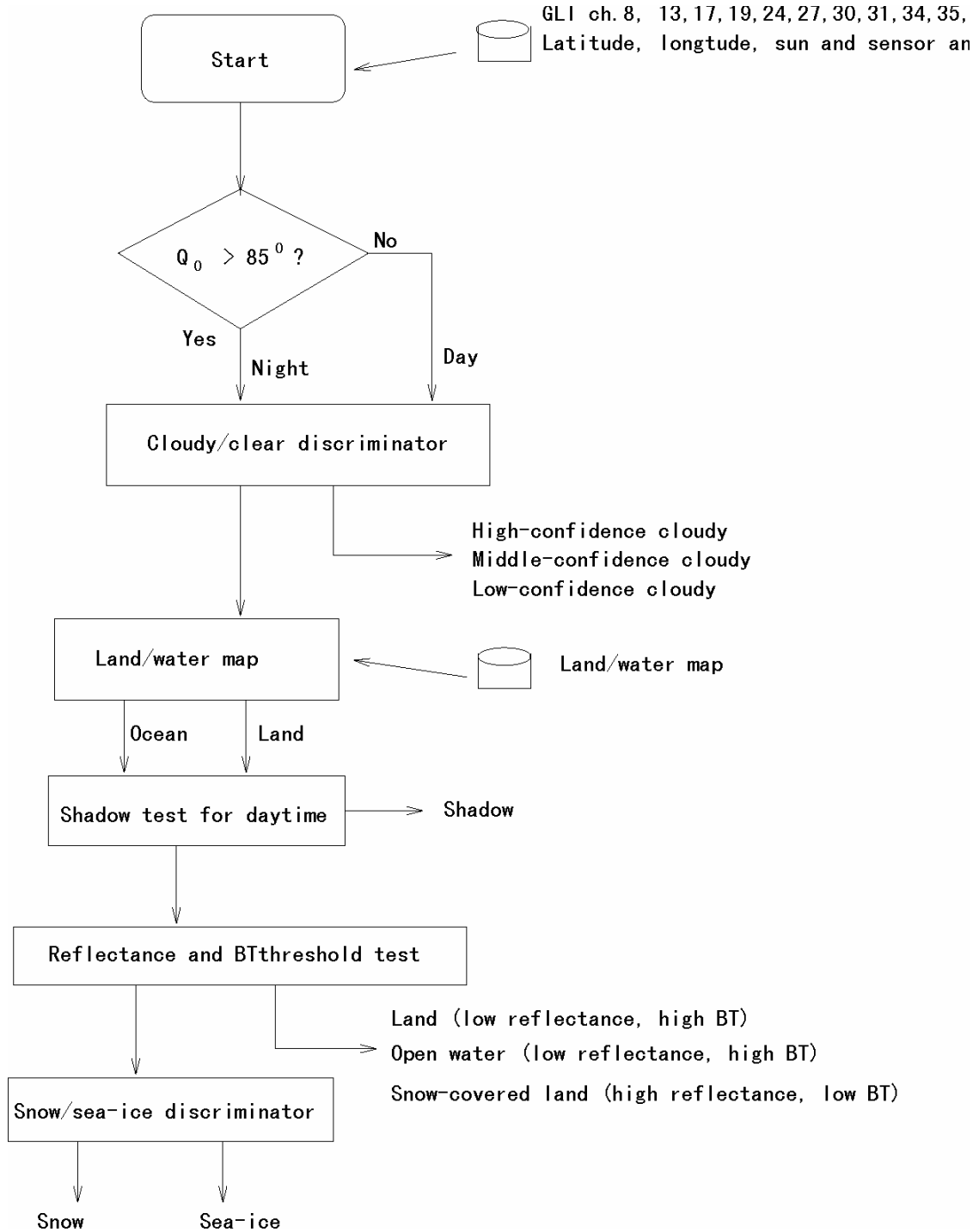


Figure 2.1  
The flow chart of algorithm for single pixel test.

Cloud shadow detection is applied for low albedo surfaces. Further work on the cloud shadow detection over snow/ice will be needed in the future.

The snow/sea-ice discriminator relies on visible and near infrared channels to distinguish bare sea ice from snow-covered sea ice. The NDII technique and the visible reflectance ratio test used in the algorithm will only be applied during daytime. Bare sea-ice appears mainly during the summer. Thus, the long daylight hours of the polar summer is an advantage since the snow/sea-ice discriminator is limited to daytime use.

An outline of the algorithm has been shown in Figure 2.1. The implementation steps of algorithm are as follows:

- I. Input GLI calibrated radiance data at level-1B and other ancillary data, including
  - A. solar and sensor position, and the location of the scan area
  - B. land/water map
  - C. GLI surface identification maps for the previous 8 or 4 days
- II. Apply cloudy/clear discriminator to set confidence flag as cloudy or clear.
  - A. determine whether the pixel is in a day or night regime
  - B. apply single cloudy/clear test to assign confidence level for each test, depending on its value relative to the threshold
  - C. determine final confidence flag, which is the maximum confidence of all applied tests
- III. Apply surface classification algorithm to classify surface into high albedo surface (snow and ice) and low albedo surface (bare land, land with vegetation and open ocean).
- IV. Apply cloud shadow test to tag shaded pixels.
- V. Apply snow/sea-ice discriminator to tag bare sea-ice and snow-covered sea-ice.
- VI. Output the results of the algorithm, which is an 8-bit word for each pixel.

The algorithm has been applied to MAS (MODIS Airborne Simulator, deployed on-board the ER-2 aircraft) data (ARMCAS, April-95 Alaska, WINCE). MAS has a spatial resolution of approximately 50 m, which is much higher than the ground resolution (1 km) of the GLI sensor. Results from these applications should aid in algorithm development. A comparison of NDSI technique and brightness temperature difference test of 10.8 and 3.7  $\mu\text{m}$  has been presented to verify the feasibility of using brightness temperature difference test instead of NDSI technique. The algorithm has been applied to high latitude areas (ARMCAS and April-

95 Alaska data) as well as to mid-latitude areas (WINCE data). It is feasible to extend this algorithm to snow-covered mid-latitude areas. Due to the absence of winter data and the  $6.7 \mu\text{m}$  channel in MAS, the temperature inversion test could not be tested by use of MAS data.

## (2) Physical and Mathematical Aspects of Algorithm

### 1. Objective

There are two main objectives of this investigation: (i) to determine whether a given FOV (field of view) is obstructed by clouds, and (ii) for cloud-free pixels to distinguish the bare sea-ice from snow-covered sea-ice. The algorithm yields an 8-bit word output for each pixel to describe the sky condition (i.e., whether the pixel is obstructed by clouds) and the surface type for a given pixel under cloud-free conditions. The surface will be classified into five possible types: snow, sea-ice, cloud shadow, land (tundra), and open ocean. When sea-ice is covered by snow (even only a few centimeters), the surface radiative characteristics will be similar to snow (Jin et al., 1994). Thus, sea-ice covered by snow will be classified as a snow surface, while only bare sea-ice is classified as sea-ice.

### 2. Background

Our development of the cloudy/clear discriminator and the snow/sea-ice discriminator for ADEOS-II/GLI has benefited from previous studies in this field (Hall et al., 1996; Ackerman et al., 1997). Since some of the GLI channels are similar to those of MODIS (The Moderate Resolution Imaging Spectrometer), we will adopt the results of previous studies in our work. Compared to AVHRR (Advanced Very High Resolution Radiometer) that has only five channels, the multiple GLI channels will allow us to extract more information about the cloud and snow/sea-ice surface in the polar regions which has been considered as a difficult remote sensing problem. However, many methods and techniques as well as related results concerning a cloudy/clear discriminator developed for the AVHRR can be employed and modified for use with the GLI.

The ISCCP (International Satellite Cloud Climatology Project) cloud masking algorithm, as described by Rossow (1989) and Rossow and Garder (1993), relies on comparing the observed radiances with their corresponding clear-sky values in two channels ( $0.6 \mu\text{m}$  and  $11 \mu\text{m}$ ). Rossow and Garder (1993) summarized the five steps employed for ISCCP cloud detection as follows: (i) space contrast test on a single infrared image; (ii) time contrast test on three consecutive visible images; (iii) accumulation of space/time statistics for infrared and visible images; (iv) construction of clear-sky composites for the infrared and visible every five days at each diurnal phase and location; and (v) radiance threshold for the infrared and visible for each pixel.

The AVHRR Processing scheme Over cLOUD Land and Ocean (APOLLO) (Kriebel and Saunders, 1988; Kriebel et al., 1989; Gesell, 1989) uses AVHRR channels 1 through 5 based on five threshold tests, i.e., a brightness temperature threshold test, the reflectance ratio of channels 2 to 1, the temperature difference between channels 4 and 5, and the spatial uniformity over ocean (Kriebel et al., 1989). A pixel is defined as cloud contaminated if it fails in any single test, so in that sense the APOLLO scheme is cloud conservative.

The NOAA CLAVR algorithm (Phase I) relies on multispectral decision, channel differences, and spatial differences, and then employs a series of sequential decision tree tests with all five channels of the AVHRR (Stowe et al., 1994). A 2 x 2 global area coverage (GAC) pixel array is used for identification in such a way, that if all four pixels satisfy just one of the cloud tests, then the array is labeled as 100% cloudy or “restored-clear,” otherwise, it is labeled as mixed or 50% cloudy. Subsequent phases of CLAVR will use dynamic thresholds and pixel by pixel classification. A cloud-contaminated pixel is radiatively *typed* as belonging to low stratus, thin cirrus or a deep convective cloud system.

Several algorithms have also been developed for cloud clearing for the TIROS-N Operational Vertical Sounder (TOVS). For example, the fifth version of the International TOVS Processing Package (ITPP-5) uses collected AVHRR and HIRS/2 (High-Resolution Infrared Sounder) to cloud-clear the HIRS/2 footprints (3 x 3 retrieval box). Several methods, such as a brightness temperature (BT) or an albedo threshold test, a BT difference test or a BT, a skin temperature difference test, and a difference test employing BT derived from AVHRR and HIRS/2, are used to determine cloudy sky condition. The nature of the cloud cover is determined in further steps. Operational GOES products by NESDIS use an array of  $n \times n$  continuous pixels and use a method similar to that of ITPP-5 (Ackerman et al., 1997).

As the high albedo of snow cover presents a good contrast with most other natural surfaces, snow cover was observed in the first image obtained from the TIROS-1 weather satellite following its launch in April 1960 (Singer and Popham, 1963), and has been mapped in the Northern Hemisphere on a weekly basis since 1966 by NOAA. A variety of sensors, including AVHRR and passive-microwave sensors, have been widely used for the detection of snow cover. Various techniques, ranging from visual interpretation, multispectral image classification, decision trees, change detection, and ratios (Kyle et al., 1978; Bunting and d’Entremont, 1982) have been developed to map snow cover with remotely sensed data. Spectral-mixture modeling is also used for subpixel classification of snow in a scene (Nolin et al., 1993; Rosenthal, 1993).

The snow-mapping algorithm (SNOMAP) developed for MODIS relies on use of an NDSI (Normalized Difference Snow Index) test and a decision rule to identify snow in each 500 m MODIS pixel (Hall et al., 1995). The use of the NDSI for snow/cloud discrimination is based

on the fact that the snow reflects visible radiation more strongly than it reflects radiation in the middle-infrared part of the spectrum, while cloud reflectance remains high in these two spectral regions. Thus, a low value of the NDSI is indicative of cloud, and a relatively higher value of snow cover. However, a visible threshold test must be conducted to separate snow cover from land/open ocean. The NDSI test is of limited value over dense forest cover, or in the presence of thin cirrus clouds. Other advanced classification techniques (Nolin et al., 1993) permit subpixel classification and improve the identification of fractional snow cover. It is likely that spectral-mixture modeling or another advanced classification technique that does not rely on thresholding could be implemented after launch of MODIS (Hall et al., 1995).

Some of the above cloud masking algorithms have been incorporated into current global cloud climatologies and have been run in an operational mode over long time periods. We have also benefited from other cloud detection studies, e.g., the algorithms developed for MODIS, in our development of a cloudy/clear discriminator for the GLI. However, due to the special difficulty associated with cloud detection over high albedo surfaces in the polar regions and the characteristics of the GLI multispectral information, some improvements to the previous algorithms have been made and used with the specific GLI channels. Since most of our data processing studies are based on MAS data and radiative transfer simulations, further improvements may be possible when data from the GLI become available.

The detection of cloud shadows is a difficult problem in the development of a proper cloudy/clear discriminator. Theoretically, they can be computed from the given view angle, solar angle, distribution of cloud edges, and cloud altitude, but it takes considerable computing time. There are two thresholds used for cloud shadow detection over land, which are based on the reflectance at channels 13 ( $0.678 \mu\text{m}$ ), 19 ( $0.865 \mu\text{m}$ ), and 24 ( $1.05 \mu\text{m}$ ):  $R_{0.865}/R_{0.678} > 0.9$ ;  $R_{1.05} < 0.12$  (Ackerman et al., 1997). Cloud shadow detection over snow is currently at an immature stage and will require substantial development beyond the scope of this project.

### 3. GLI Characteristics

The GLI has 36 channels with channels 1–29 in the visible and near-infrared (NIR), and the rest of the channels in the thermal-infrared ranging from 3 to  $12 \mu\text{m}$ . The specifications of the GLI channels used here are shown in Table 2.2. There are some channels that are similar among GLI, MODIS and AVHRR (see Table 2.2). Due to this similarity, our work is benefiting from previous experience and results by others in algorithm development.

Table 2.2 GLI channels to be used in the algorithm

GLI channel	$\lambda$ ( $\mu m$ )	$\Delta \lambda$ ( $\mu m$ )	GR (km)	Purpose	MODIS channel	AVHRR channel	MAS channel
8	0.545	0.01	1	surface classification, cloudy/clear and snow/sea-ice discriminator	4	1	1
13	0.678	0.01	1	surface classification, cloud shadow, cloudy/clear and snow/sea-ice discriminator	1	1	2
17	0.763	0.008	1	cloudy/clear discriminator	15		5
19	0.865	0.01	1	snow/sea-ice discriminator and cloud shadow	2	2	7
24	1.05	0.02	1	cloud shadow, snow/sea-ice discriminator			9
27	1.38	0.04	1	cloudy/clear discriminator	26		15 (1.88 $\mu m$ )
30	3.715	0.33	1	cloudy/clear discriminator	20	3	30
31	6.70	0.50	1	cloudy/clear discriminator	27		
34	8.60	0.50	1	cloudy/clear discriminator	29		42
35	10.8	1.0	1	cloudy/clear discriminator	31	4	45
36	12.0	1.0	1	cloudy/clear discriminator	32	5	46

Figure 2.2 shows simulated planetary albedoes for various types of surfaces and water/ice clouds in the 0.3-2.5  $\mu m$  spectral range. The location and bandwidth of GLI channels 1-29 are also shown in Figure 2.2. The 36 GLI channels offer the opportunity to use multispectral approaches for cloud detection. The analysis of cloud cover in the polar regions from satellite data is more difficult than at lower latitudes because the visible and thermal contrasts between the cloud cover and the underlying surface are frequently quite small. However, a notable difference between cloud and snow can be found at 1.6  $\mu m$ . Based on this information, the NDSI technique could be used to distinguish clouds from snow surfaces (Hall et al., 1995). Unfortunately, the ground resolution of GLI channel 28 (1.64  $\mu m$ ) has been designed as 250 m,

rather than 1 km which is the ground resolution for all channels we used here. So we cannot use the NDSI technique in this algorithm. Another brightness temperature difference test using channel 30 ( $3.7 \mu\text{m}$ ) and channel 35 ( $10.8 \mu\text{m}$ ) will be adopted for the cloudy/clear

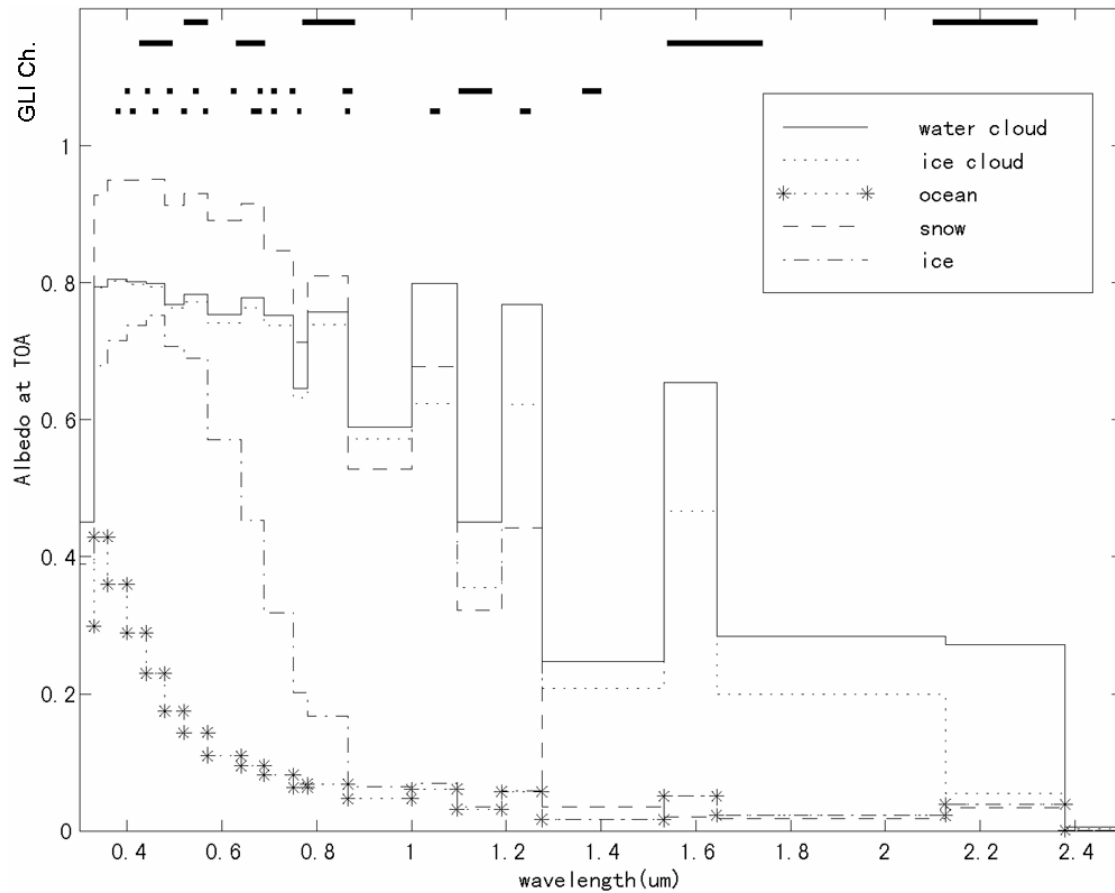


Figure 2.2  
The planetary albedoes of various types of surfaces and clouds in the spectral range between  $0.3$  and  $2.5 \mu\text{m}$  for solar zenith angle  $\theta = 60^\circ$ . The location and bandwidth of GLI channels 1-29 are also shown at the top part of the figure with black dots or lines.

discriminator instead of the NDSI technique.

The cloudy/clear discrimination can be accomplished using GLI channels 8, 13, 19, 24, 27, 30, 31, 34, 35 and 36. These channels are employed for detecting low cloud, high cloud, and cloud shadow.

The principal differences in planetary albedo between snow and ice occur at NIR bands ( $0.6$ - $1.2 \mu\text{m}$ ), as shown in Figure 2.2. As a result of the strong absorption of sea ice in the NIR, the reflectance over ice is much lower than over snow. This difference provides the theoretical basis for the snow/sea-ice discriminator. Based on the different albedo between snow and sea-ice, GLI channels 8, 13, 19 and 24 are used for snow/sea-ice discrimination. We use a new index called the NDII (Normalized Difference Ice Index) as our main test for snow/sea-ice discrimination. The NDII test will be used only during day time. Fortunately, sea-ice is covered by snow most of the year. Bare sea-ice appears primarily in the summer season. The

bright polar summer offers a possibility to apply the NDII-based snow/sea-ice discriminator which is effective only during day time.

GLI channels with 1 km ground resolution will be used for this algorithm. GLI will provide measurements at the same position every four days. The four-day recovery schedule is also used to test for temporal uniformity for the confirmation of surface type.

MAS data are used for the validation of the algorithm. The MAS data set used in this study includes ARMCAS (Arctic Radiation Measurement in Column Atmosphere-surface System), ALASKA\_April\_95 (i.e., snow, glaciers and sea-ice measurements, March-April 1995, in north central Alaska), and WINCE (WINTER Cloud Experiment, Jan. 23 to Feb. 13, 1997, over the Great Lakes area) data. These data sets provide the opportunity to apply and test the cloud detection and surface identification algorithm over polar and mid-latitude snow-covered areas.

#### 4. Physical aspects of the algorithm

This algorithm is different from the MODIS cloud-mask algorithm, which is based on a given surface condition. We have designed an algorithm which is independent of surface conditions so that it will be applicable to the variable surface conditions encountered in the polar regions during the spring, summer and autumn. We also employ multispectral ratios and threshold-based methods to obtain a simple and effective algorithm.

The algorithm consists mainly of the cloudy/clear discriminator (CTSK1a), the snow/sea-ice discriminator (CTSK1b), and a surface classification. The last component goes beyond the tasks CTSK1a and CTSK1b that we committed to do as part of this project. We offer this simple surface classification algorithm to help identify high-albedo ocean areas from the clear pixels. The snow/sea-ice discriminator algorithm will be implemented only for these high-albedo ocean areas, to distinguish the bare sea-ice from snow-covered sea-ice. A flow chart of the algorithm for a single pixel test is shown in Figure 2.1. The algorithm will start with single-pixel (1 km FOV) tests. For pixels with low-confidence cloud, a spatial coherence test may be applied on 3 x 3 pixel segments to improve the confidence of the cloud detection.

For nomenclature, we shall denote the satellite-measured radiance as  $I_{\lambda}$  and the normalized reflectance as  $R_{\lambda}$ , and we shall refer to the infrared radiance as brightness temperature (equivalent blackbody temperature determined using the Planck function) denoted as  $BT_{\lambda}$ . Subscripts refer to the wavelength in  $\mu m$  at which the measurement is made. We define the normalized reflectance as:

$$R_{\lambda} = \frac{\pi I_{\lambda}}{S_{\lambda} \cos \theta_0}$$

where  $S_{\square}$  is the extraterrestrial solar irradiance. A threshold will be set for each single test based on the normalized reflectance  $R_{\square}$  when the channel wavelength is less than  $3 \mu m$ , and based on brightness temperature when the channel wavelength is larger than  $3 \mu m$ .

#### 4.1 The Cloudy/Clear Discriminator

The detection of clouds in the polar regions or in snow-covered mid-latitude areas is difficult because of insufficient albedo contrast between the cloud and the underlying snow or sea ice surface. Since snow and ice are considerably more reflective in the visible than in the NIR part of the spectrum and the reflectance of clouds remains high in the NIR, the Normalized Difference Snow Index (NDSI) technique based on a channel at  $1.64 \mu m$  is used to distinguish snow from clouds (Hall et al., 1995). Due to the limitation of ground resolution of GLI channel 28 ( $1.64 \mu m$ ), we cannot use the NDSI technique in our cloudy/clear discriminator. A brightness temperature difference ( $BT_{10.8}$  and  $BT_{3.7}$ ), which was used only in night mode in our earlier version, will be used also during daytime, instead of the NDSI technique. A comparison between the NDSI technique and the brightness temperature difference, based on MAS data, has demonstrated the usefulness of the brightness temperature difference test. Additionally, we use the  $1.38 \mu m$  channel for thin cirrus detection during daytime and we use four thermal channels ( $3.7$ ,  $8.6$ ,  $11$ , and  $12 \mu m$ ) for cloud detection during night.

Under clear-sky conditions, strong surface temperature inversions often exist in the polar regions during winter. Clouds generally tend to inhibit the formation of the inversion. Therefore, the presence of a strong, low-level temperature inversion is a good indication of a clear sky condition. The  $6.7$  and  $10.8 \mu m$  channels will be used for temperature-inversion detection in polar winter for both the daytime and the nighttime modes. A detailed analysis of the temperature-inversion test will be deferred (see below).

A combination of these tests constitutes the main part of the algorithm, since none of them can be considered as a perfect technique for detecting all kinds of clouds under different environmental conditions. For example, some are more reliable for low-cloud detection, while others are better for high-cloud detection. The result of each single test is expressed as a *confidence* level ranging from 1 (cloudy pixel with high confidence) to 0 (clear pixel). The final confidence flag will be assigned by considering the maximum confidence of all tests applied. This is called the cloud conservative approach.

A common result of the cloudy/clear discrimination from this algorithm is either high-confidence cloudy or clear, except for cases in which there are some low-confidence clouds at cloud boundaries, or thin, low, or small clouds exist. In these cases, spatial and/or temporal continuity tests need to be conducted. The cloudy/clear discrimination algorithm has a daytime

mode and a nighttime mode depending on the solar zenith angle. *Daytime* is defined by limiting the solar zenith angle to  $\theta_0 < 85^\circ$ . The daytime mode includes brightness temperature difference (using the 3.7 and the 10.8  $\mu\text{m}$  channels) and the 1.38  $\mu\text{m}$  channel thin cirrus tests; and the nighttime mode includes infrared brightness temperature difference tests, using channels at 3.7 and 10.8  $\mu\text{m}$ . The temperature-inversion test is also included in both the daytime and the nighttime modes. Figure 2.3 shows a flow chart of the cloudy/clear discriminator algorithm.

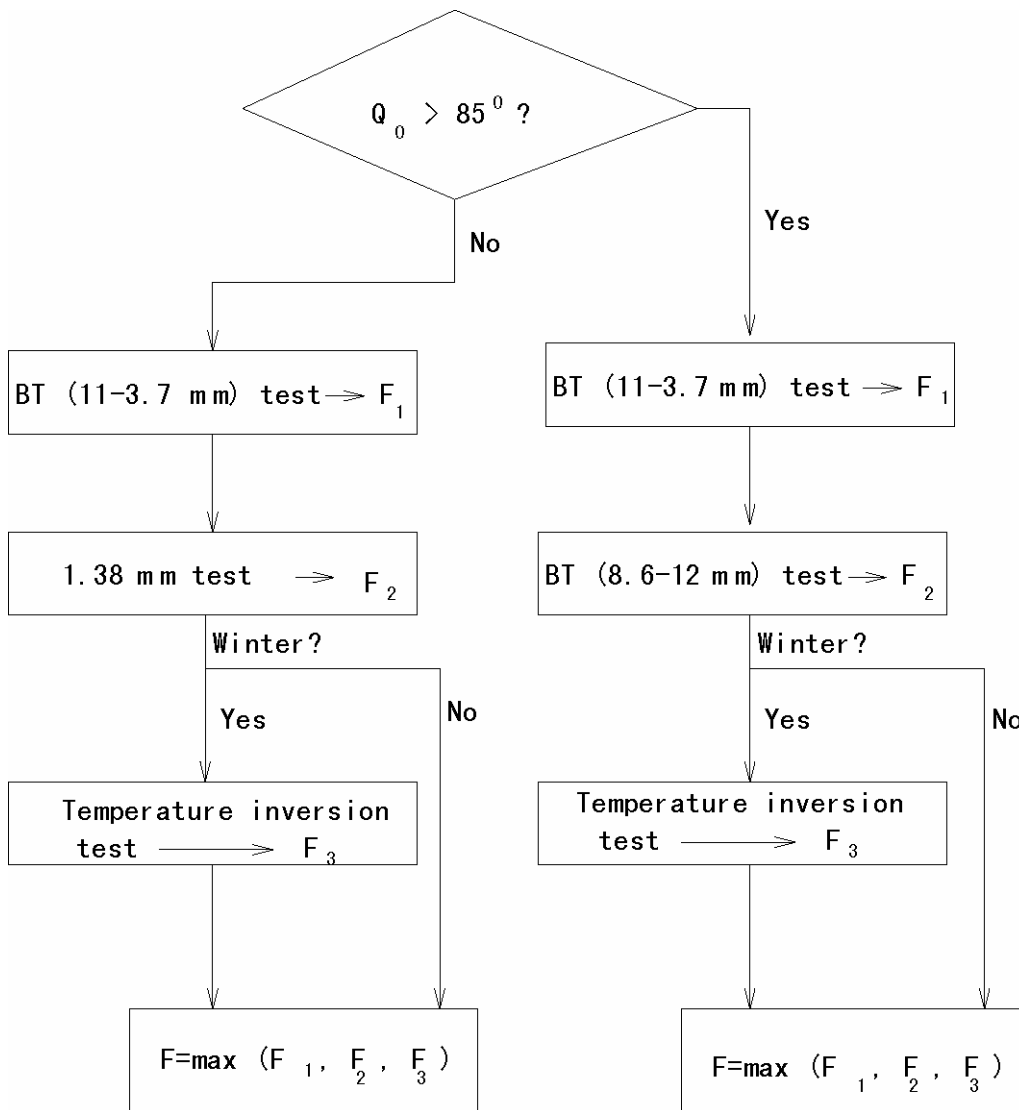


Figure 2.3  
The flow chart of cloudy/clear discriminator.  $F_1$ ,  $F_2$ ,  $F_3$ , and  $F$  are the confidence levels for individual test and final result, respectively.

#### 4.1.1 Brightness Temperature Difference Test ( $BT_{10.8}$ and $BT_{3.7}$ )

At high latitudes, infrared window tests based on satellite-measured radiances are difficult due to the cold surface, and especially the small temperature contrast between cloud and snow surface in winter. However, a nighttime polar (Antarctic) cloud/surface discrimination algorithm has already been applied by Yamanouchi et al. (1987). This algorithm is based upon the brightness temperature difference between the AVHRR 3.7 and 11  $\mu m$  channels and between the AVHRR 11 and 12  $\mu m$  channels.

GLI channel 30 (3.7  $\mu m$ ) measures radiances in the window region near 3.5-4  $\mu m$ , so we can use GLI channels 30 and 35 (10.8  $\mu m$ ), another window region, to detect the presence of clouds. In particular we can detect partial cloudiness or thin cloud cover at night based on the difference between  $BT_{10.8}$  and  $BT_{3.7}$ . The MAS data at 3.7  $\mu m$  (channel 31) and 11.0  $\mu m$  (channel 45) will be used for validation and determination of the threshold. Another method for determining the threshold is based on modeling results. Small or negative differences  $BT_{10.8} - BT_{3.7}$  are observed only for cases when an opaque scene (such as thick cloud or the surface) fills the field of view of the sensor. Negative difference  $BT_{10.8} - BT_{3.7}$  occurs at night over extended clouds due to the lower cloud emissivity at 3.7  $\mu m$ . Large negative difference  $BT_{10.8} - BT_{3.7}$  occurs during daylight hours because of the large reflection of solar radiance at 3.7  $\mu m$ .

This test will be used in both daytime and nighttime modes. Because of the reflection of solar energy at 3.7  $\mu m$  during daytime, the thresholds used for daytime and nighttime modes are quite different.

#### 4.1.2 Thin Cirrus Test (1.38 $\mu m$ ) channel

The detection of thin cirrus is a challenging problem, especially in polar regions. Fortunately, GLI channel 27 (1.38  $\mu m$ ) provides an opportunity to detect the presence of thin cirrus in the upper troposphere under daytime viewing conditions by use of reflectance thresholds (Gao et al., 1993). The premise of this test comes from the strong water vapor absorption in the 1.38  $\mu m$  region. Therefore, most of the earth's surface is obscured at this channel. With relatively little of the atmosphere's moisture located high in the troposphere, high clouds appear bright. Simple low and high reflectance threshold will be used to separate thin cirrus from clear scenes as well as scenes with thick cloud. The MAS 1.88  $\mu m$  channel will be used in conjunction with theoretical simulations for validation and for determining the threshold, because strong water vapor absorption exists in both the 1.38  $\mu m$  channel and the 1.88  $\mu m$  channel.

#### 4.1.3 Brightness Temperature Difference Test ( $BT_{8.6} - BT_{12}$ )

The  $1.38 \mu m$  channel thin cirrus test can not be used for cloudy/clear discrimination during the dark winter time in the polar regions. Instead we have to use infrared channels for this purpose. Because the sensitivity of the refractive index for ice and water vapor is different in the window region, their absorption peaks are in opposite halves of the window region around  $8-12 \mu m$ . The difference in brightness temperature between GLI channels 34 ( $8.6 \mu m$ ) and 36 ( $12 \mu m$ ),  $BT_{8.6} - BT_{12}$ , can therefore be applied during night time to discriminate between high level clouds and cloud-free conditions.

#### 4.1.4 Temperature Inversion Test ( $BT_{6.7}$ and $BT_{6.7} - BT_{10.8}$ )

Normally, there is strong temperature inversion under clear-sky conditions in polar winter (Curry et al., 1996). Thus, a temperature-inversion test is another way to achieve cloudy/clear discrimination. Infrared channels whose weighting functions peak low in the atmosphere will often have a larger BT than a window channel (e.g.,  $BT_{6.7} - BT_{10.8}$ ). In clear sky situations, the  $6.7 \mu m$  radiation measured by the satellite instrument is emitted by water vapor in an atmospheric layer located approximately between 200-500 hPa (Soden and Bretherton 1993; Wu et al., 1993), while  $6.7 \mu m$  radiation emitted by the surface or low clouds is absorbed in the atmosphere and is not sensed by the satellite instruments. On the contrary, the measured  $10.8 \mu m$  radiation under clear sky originates primarily at the surface. Strong inversions in polar winter under clear-sky conditions lead to large negative differences in  $BT_{10.8} - BT_{6.7}$  (below  $-10 K$ ) that can be used to detect cloud-free conditions. The GLI channels 31 ( $6.7 \mu m$ ) and 35 ( $10.8 \mu m$ ) will be used for this test.

#### 4.1.5 Confidence Flags

Almost all tests mentioned above rely on the pre-defined thresholds. Instead of a single threshold, the user can obtain information about how much confidence can be placed in the results. The confidence of every single test is assigned a value between 0 and 1, representing increasing confidence that clouds are present. Figure 2.4 is a graphical representation of how a confidence level is assigned for a test. As shown in Figure 2.4, an observational value greater than  $\gamma$  corresponds to high confidence that a cloud is present and is assigned a confidence level of 1. An observed value less than  $\alpha$  is clear and will be assigned a confidence level of 0. These high-confidence cloudy and clear thresholds,  $\gamma$  and  $\alpha$  respectively, are determined from observations and/or theoretical simulations. Observational values between  $\alpha$  and  $\gamma$  are assigned a confidence level between 0 and 1. Assignment is based on a linear interpolation.

Each of the tests mentioned above returns a confidence level ranging from 1 (high confidence cloud) to 0 (clear-sky). Based on the cloud conservative approach, we set final

confidence level as the maximum confidence level of all applied tests (shown in Figure 2.3). The final confidence level will determine the final flag as cloudy or clear for the output file (bit 2-1).

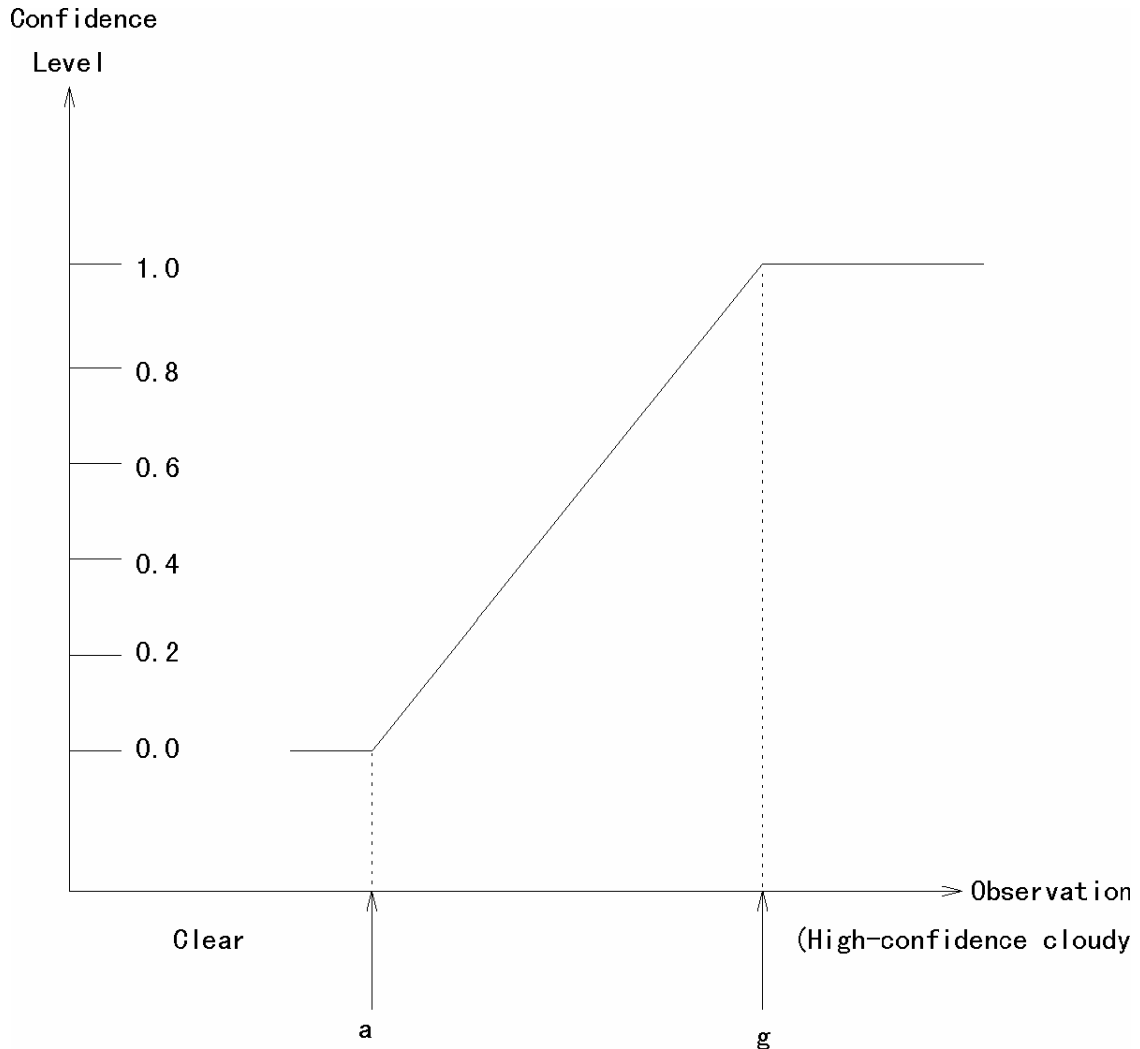


Figure 2.4  
A graphical representation of confidence level.

#### 4.2 Theoretical Description of the Snow/Sea-ice Discriminator

Snow exhibits strong reflectance in the visible region and strong absorption in the NIR region. The NDSI technique has been successfully applied to distinguish snow from clouds as discussed in previous sections. Sea ice has characteristics similar to snow. It is more difficult to distinguish sea-ice from snow than detecting clouds over snow. However, there is a difference in albedo between snow and sea-ice in the region of 0.6-1.2  $\mu\text{m}$  (see Figure 2.1). Due to the strong absorption of sea-ice, the planetary albedo of sea-ice drops rapidly at 0.6  $\mu\text{m}$ , while snow maintains relatively high albedo until 1.2  $\mu\text{m}$ . Based on this characteristic, we

employ the NDII technique (Normalized Difference Ice Index) (see section 4.2.1) as the main test for snow/sea-ice discrimination. A reflectance ratio test (see section 4.2.2) is an auxiliary test used in the snow/sea-ice discriminator algorithm. The two tests in the snow/sea-ice discriminator will only be used during daytime.

#### 4.2.1 Normalized Difference Ice Index (NDII) Test

Under clear-sky conditions, the principal differences in planetary albedo between snow and sea-ice occur in the NIR region between 0.6 and 1.2  $\mu m$ , as shown in Figure 2.2. Snow and sea ice have similar reflectance for wavelengths shorter than 0.6  $\mu m$ . As a result of the strong sea-ice absorption in the NIR, the reflectance over sea-ice is much lower than over snow in that wavelength region. Thus channel 24 (1.05  $\mu m$ ) can be used to distinguish snow from sea ice.

In addition, we also need to employ another band (0.5-0.7  $\mu m$ ) to distinguish ocean from snow/sea-ice. Since ocean has lower albedo than snow/sea-ice in this visible region (see Figure 2.2), GLI channel 8 (0.545  $\mu m$ ) can be used for the separation of snow/sea-ice and ocean.

Actually, there are plenty of melt ponds on the sea ice due to the melting during summer. The visible radiances for such cases will have values between that corresponding to the sea-ice case and that corresponding to the open-ocean (water) case. However, albedo of water is low at both channel 8 (0.545  $\mu m$ ) and channel 24 (1.05  $\mu m$ ), while albedo of sea ice is high at channel 9 and low at channel 24, and albedo of snow is high at both channel 8 and channel 24 (see Figure 2.2). We then define a snow/sea-ice discriminator using NDII that is similar to the case of NDSI:

$$NDII = \frac{R_{0.545} - R_{1.05}}{R_{0.545} + R_{1.05}}$$

where  $R_{0.545}$  and  $R_{1.05}$  are the normalized reflectances of channels 8 and 24, respectively. A reference radiance at channel 13 (0.678  $\mu m$ ) is required to distinguish snow from dark surfaces. For open ocean, the reference radiance is always low. When the reference radiance is high and the NDII is below a pre-defined value threshold, the current pixel is covered by snow. When the reference radiance is high and the NDII is larger than this threshold value, the pixel is covered by sea ice.

#### 4.2.2 Reflectance Ratio Test

The reflectance ratio test employs the ratio of satellite-measured radiance between channels 19 (0.865  $\mu m$ ) and 13 (0.678  $\mu m$ ) (i.e.,  $R_{0.865}/R_{0.678}$ ). This test is based on the fact that the spectral reflectances at these two wavelengths are similar over snow or water (ratio is near 1) and different over sea-ice.

### 4.3 Surface Classification

There is a simple surface classification included in the algorithm. It will be applied to all clear pixels tagged by the cloudy/clear discriminator. Visible and infrared (needed during night time) threshold tests can be applied to discriminate high albedo surfaces from low albedo surfaces. We use GLI channels 8 ( $0.545 \mu m$ ) and 35 ( $11 \mu m$ ) for visible and infrared threshold tests, respectively. The land and ocean area will be determined by the land/water map. Thus, the classification of four types of surface (open ocean, land, snow-covered land, and snow/sea-ice covered ocean) can be accomplished by using two threshold tests and the land/water map. It is necessary to tag the snow/sea-ice-covered ocean area prior to applying the snow/sea-ice discriminator.

## C. Practical Considerations

### (1) Programming Requirements

Table 3.1 provides information about the software generated from this algorithm.

Table 3.1 Program Requirements

Program Memory	400 KBytes
Program Size	100 KBytes
Required Channels	8,13, 17, 19,24,27,30,31,34,35,36
Necessary/Ancillary Data	land/water map
Expected Disk Volume	5 MBytes
Special Programs or Subroutines	mask.f
Thresholds list	thresholds.inc

### (2) Calibration and Validation

#### 1. Cloudy/clear Discriminator for MAS data

For the cloudy/clear discriminator there are two modes applied during daytime and nighttime, respectively. A brightness temperature difference test using channels at  $10.8$  and  $3.7 \mu m$  is used for both daytime and nighttime modes to distinguish cloud from snow. In addition, a  $1.38 \mu m$  channel test and a test employing the brightness temperature difference between the  $8.6$  and the  $12 \mu m$  channels are used to detect the presence of thin cirrus in both daytime and nighttime modes, respectively. Since nighttime MAS data are not available, we have used the infrared data obtained during daytime data for validation and improvement of the algorithm. Because the threshold of the daytime mode is quite different from that of the nighttime mode, MAS data cannot be used to establish the correct nighttime threshold.

### 1.1 Comparison between NDSI test and $BT_{11} - BT_{3.7}$ test

Figure 3.1 shows the results from one scene of WINCE data using the NDSI test and the brightness temperature difference test. The scene used is the observation made on February 9, 1997 over Lake Erie. We use the MAS channel at  $1.88 \mu m$  instead of GLI channel at  $1.38 \mu m$  for the thin cirrus test because MAS does not have a channel at  $1.38 \mu m$  and there is strong water vapor absorption at both the  $1.38 \mu m$  and the  $1.88 \mu m$  channels. High radiance at the  $1.38 \mu m$  channel ( $1.88 \mu m$  channel of MAS) indicates the presence of high level cloud (including thin cirrus cloud). For the left panel of Figure 3.1, we used the NDSI test as well as the  $1.88 \mu m$  channel test for the cloudy/clear discrimination. For the right panel of Figure 3.1, we used the test based on the brightness temperature difference between channels at 11 and  $3.7 \mu m$  as well as the  $1.88 \mu m$  channel test for the cloudy/clear discrimination. The different colors used in Figure 3.1 represent the results of cloudy/clear discrimination (see Table 3.2). Comparing the two panels in Figure 3.1, one finds that the difference between the two images (i.e. the two panels in Figure 3.1) is less than 10%. This indicates that the brightness temperature difference test may generally work as well as the NDSI test. Therefore, we can use the brightness temperature difference test as the main test instead of the NDSI test for cloudy/clear discrimination.

Table 3.2 Description of colors in cloud mask image

color	meaning
red	snow over ocean
blue	sea ice
yellow	land
green	high confidence cloud
sea green	middle confidence cloud
coral	low confidence cloud
magenta	snow over land
cyan	water (open ocean)

### 1.2 Comparison between $1.38 \mu m$ test and $BT_{8.6} - BT_{12}$ test

In cloudy/clear discriminator, we use the  $1.38 \mu m$  test for the daytime mode and the test employing the brightness temperature difference between the  $8.6$  and  $12 \mu m$  channels for nighttime modes. These two tests offer the potential to improve the detection of thin cirrus. Here we show a comparison between these two tests for a scene of the MAS ARMCAS data. This scene obtained on June 11, 1995 over the North Slope of Alaska. Figure 3.2 shows the cloud mask resulting from use of the  $1.38 \mu m$  test, the  $BT_{8.6} - BT_{12}$  test, and the  $BT_{11} - BT_{3.7}$

test, respectively. The left panel of Fig. 3.2 corresponds to the  $1.38 \mu\text{m}$  test for the daytime mode, the middle panel corresponds to  $\text{BT}_{8.6} - \text{BT}_{12}$  test for the nighttime mode, and the right panel corresponds to  $\text{BT}_{11} - \text{BT}_{3.7}$  test for both daytime mode and nighttime mode. Cirrus cloud should have a high value at  $1.38 \mu\text{m}$  and  $\text{BT}_{8.6} - \text{BT}_{12}$ . At the top of image, there are some water clouds detected by  $1.38 \mu\text{m}$  test, but not by  $\text{BT}_{8.6} - \text{BT}_{12}$  test. It implies that  $1.38$

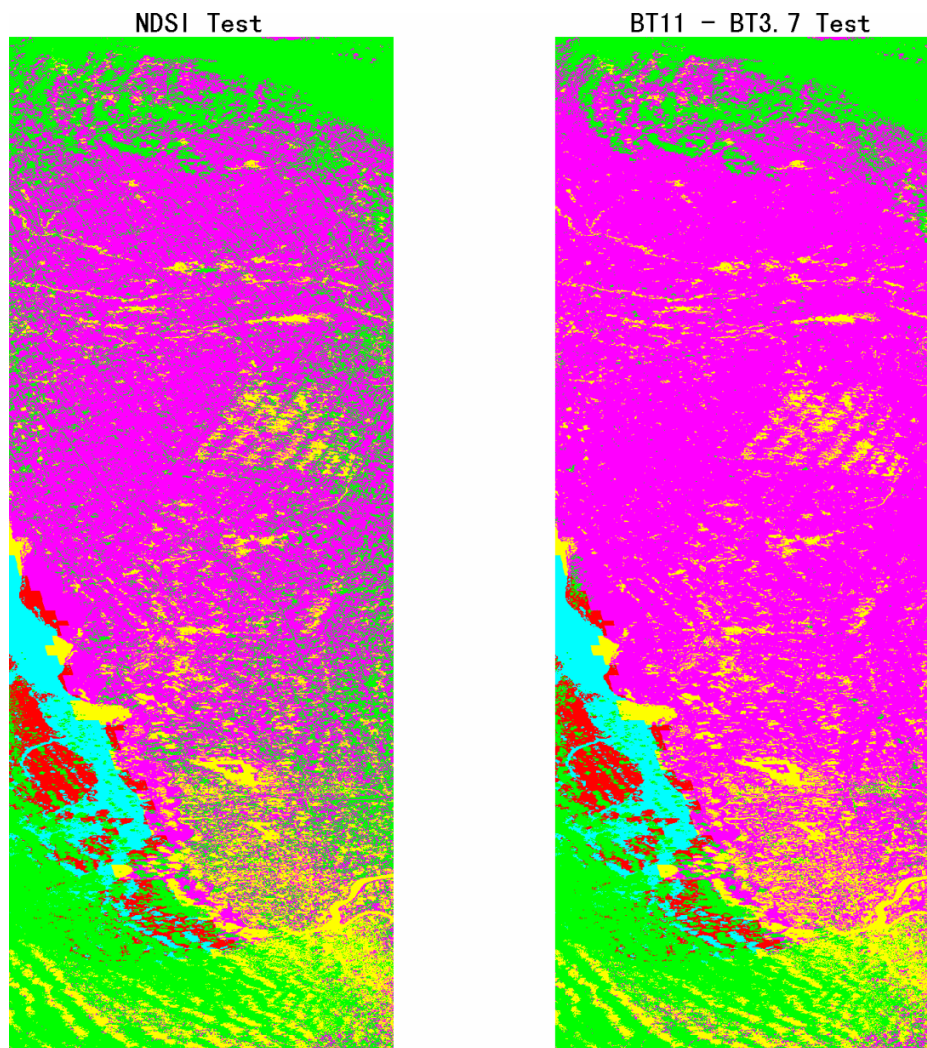


Figure 3.1

An example of a cloudy/clear discriminator image derived from MAS WINCE data over the Lake Erie on Feb. 9, 1995 (track 3). The left panel is for the NDSI test. The right panel is for the brightness temperature difference test.

$\mu\text{m}$  test is not only sensitive to cirrus cloud, but also to some thick low cloud. These water clouds have also been detected by  $\text{BT}_{11} - \text{BT}_{3.7}$  test which is a main test for both daytime and nighttime mode (See right panel of Fig. 3.2). Figure 3.3 shows two images of cloud mask results using the same data as shown in Fig. 3.2 for daytime mode (left panel) and nighttime mode (right panel). From Fig.3.3, we have found that both daytime mode and nighttime mode yield similar cloud mask images.

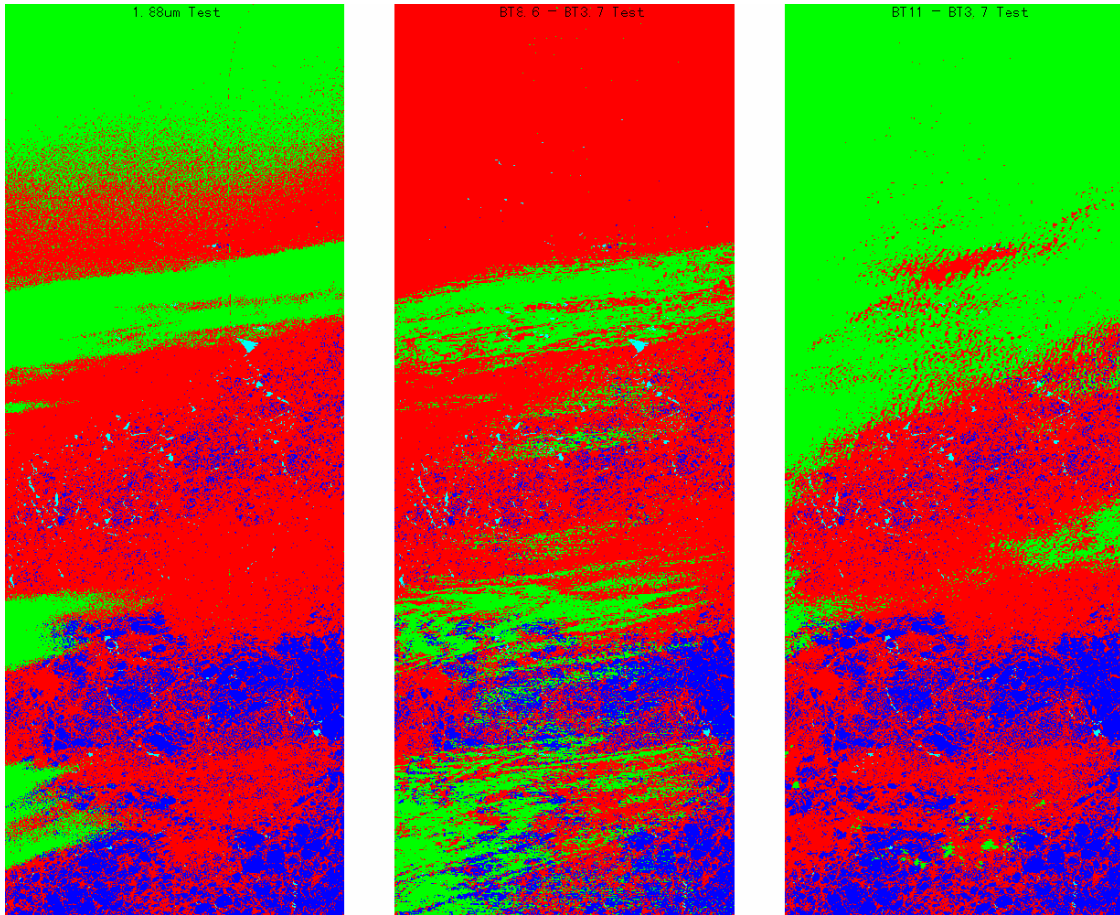


Figure 3.2

An example of a cloudy/clear discriminator image derived from MAS ARMCAS data collected over the North Slope of Alaska on June 11, 1995 (track 4). The left panel is for the  $1.38 \mu\text{m}$  test, the middle panel is for the  $BT_{8.6} - BT_{12}$  test, and the right panel is for  $BT_{11} - BT_{3.7}$  test.

From the results of the two cases in Figs. 3.1 and 3.2, we have found that we can successfully carry out cloudy/clear discrimination using  $BT_{11} - BT_{3.7}$  test instead of NDSI test in daytime mode. We have also found that both the daytime and the night modes of the cloudy/clear discriminator algorithm seem to work well over snow/ice surfaces in the polar regions as well as in mid-latitude areas.

## 2. Snow/sea-ice Discriminator for MAS data

Under clear-sky conditions, snow/sea-ice discrimination over ocean area will be based on the NDII test and the ratio-threshold test. Validation of this algorithm has been carried out by using MAS data obtained in the ARMCAS and Alaska-April-95 campaign. MAS channels 2 ( $0.653 \mu\text{m}$ ) and 9 ( $0.945 \mu\text{m}$ ) are employed in the NDII test to mimic GLI channels 8 ( $0.545 \mu\text{m}$ ) and 24 ( $1.05 \mu\text{m}$ ). The reflectance ratio between MAS channels 2 ( $0.653 \mu\text{m}$ ) and 5

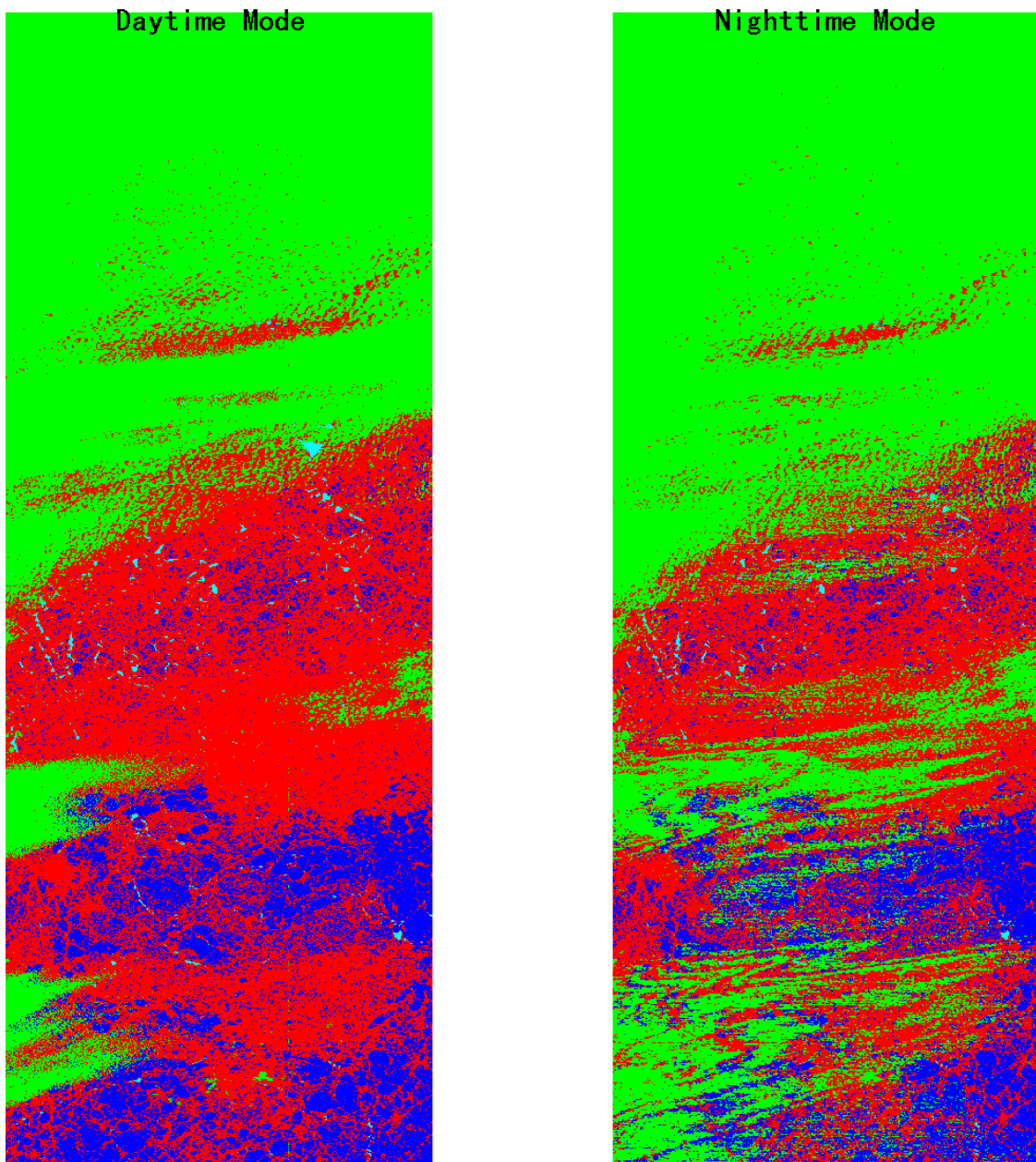


Figure 3.3  
 An example of a cloud mask image derived from MAS ARM-CAS data over North Slope of Alaska on June 11, 1995 (track 4). The left panel is for daytime mode, and right panel is for nighttime mode.

(0.781  $\mu\text{m}$ ) is also employed to mimic GLI channels 13 (0.678  $\mu\text{m}$ ) and 19 (0.865  $\mu\text{m}$ ), as the second test for discriminating snow from bare sea-ice.

One case is presented here to indicate that the NDII test and the ratio test can be used to discriminate snow from bare sea-ice. This scene is an observation made on April 8, 1995 (track 14) over the Bering Sea (Fig. 3.4). This figure shows the ice mask combining the NDII

test and ratio test, The algorithm is sea-ice conservative. The colors in image have been described in Table 3.2.

#### cloud mask and snow/sea-ice discriminator

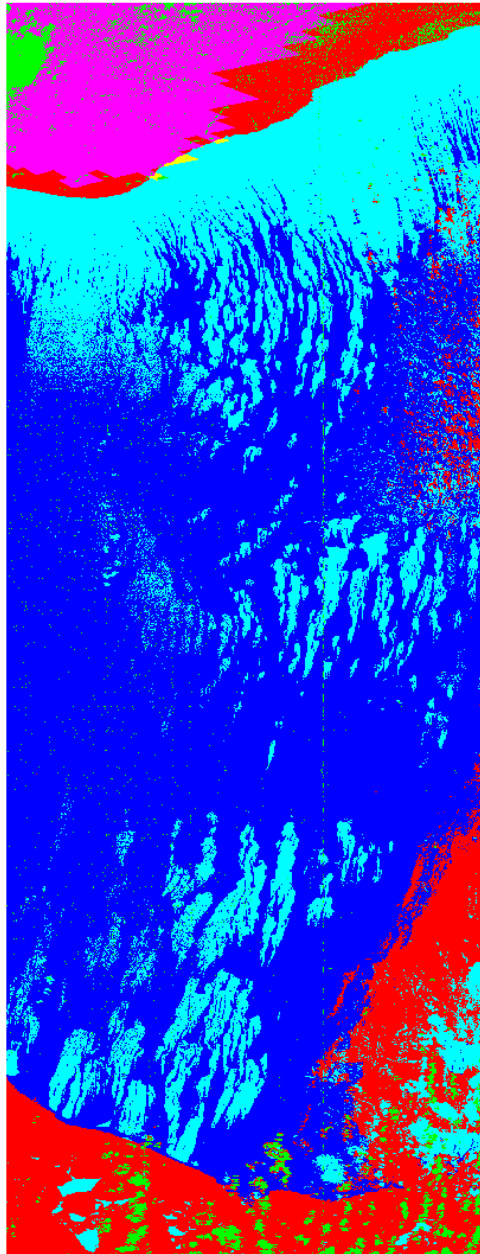


Figure 3.4

An example of snow/sea-ice discriminator derived from MAS data over the Bering Sea of Alaska on April 8, 1995 (track 14). This shows the results of the cloud mask and snow/sea-ice discriminator.

Prior to generating the sea ice mask, pixels with high confidence cloud occurrence (green area) are identified based on the  $BT_{11} - BT_{3.7}$  test and the  $1.88 \mu\text{m}$  test. Then, a reference channel (MAS channel 2, corresponding to GLI channel 13) is used to discriminate sea ice from open water. Finally, the NDII and the ratio tests are applied to mark the bare sea ice

surface (blue area). The cyan area is the open ocean, caused by ice lead or pond after the snow over sea ice melts, when the reflectance in MAS channel 2 is low. The red area is snow-covered area when the reflectance in channel 2 is high. In Fig. 3.4, St. Lawrence Island covered by snow is just at the top of panel. There is open water along the coast. Near the coast, there are many floating ice sheets. This is a scene under clear-sky condition, except for a small amount of cumulus clouds over the ocean surface. Snow-covered sea-ice was present at the bottom of the scene.

From the case discussed in this section, it is obvious that the sea-ice can be discriminated from snow and water by the algorithm described above.

### (3) Quality Control and Diagnostic Information

### (4) Exception Handling

### (5) Constraints, Limitations, Assumptions

According to the requirements of ADEOS-II/GLI/CTSK1a and ADEOS-II/GLI/CTSK1b, an algorithm has been developed for cloudy/clear discrimination and snow/sea-ice discrimination. The cloudy/clear discriminator consists of a daytime as well as a nighttime mode. The  $BT_{11} - BT_{3.7}$  test has been successfully and effectively used in the daytime mode of the cloudy/clear discriminator instead of NDSI technique due to the lack of  $1.64 \mu m$  channel. The  $1.38 \mu m$  channel test, which is important for the detection of thin cirrus, has been included in the daytime mode. In the nighttime mode, the  $BT_{8.6} - BT_{12}$  brightness temperature difference test based on the different refractive indexes for ice and water is available to detect cirrus cloud. During polar winter, a temperature inversion test is included into both the daytime and the nighttime modes to improve the capability of the cloud detection.

The snow/sea-ice discriminator is a daytime only mode. The so-called NDII technique and the reflectance-ratio approach have been used in the algorithm. GLI channel 24 ( $1.05 \mu m$ ) is an important channel for discriminating snow from bare sea ice. The rapid decline of ice reflectance in the  $0.6-1.2 \mu m$  region is the basis for the snow/sea-ice discriminator algorithm. Applications to the MAS data set reveal that the NDII is an effective method for the separation of sea-ice and snow/open-water.

The basic features of the algorithm may be summarized as follows:

- (i) The cloud detection algorithm is designed to work independently without considering surface conditions and to be valid for both polar regions and snow-covered mid-latitude regions. The threshold for each test applied in this algorithm has the same value for

different surfaces. Thus, the cloud-contaminated pixels can be detected before the surface condition is known.

- (ii) The algorithm is based on pre-defined thresholds. The results of the cloudy/clear discriminator are indicated as 4 levels of confidence with regard to whether a pixel is considered to be cloudy. This algorithm is constructed to be cloud-conservative, minimizing false cloud detection but missing clouds that resemble clear conditions.
- (iii) The snow/sea-ice discriminator works only during daytime. Fortunately, bare sea-ice occurs primarily in summer. Bright polar summers will offer the opportunity to use the snow/sea-ice discriminator for extended periods of time.
- (iv) The nighttime mode is necessary during polar winter. The thresholds of the infrared channels used in the nighttime mode should be determined based on nighttime observational data. Due to the lack of nighttime data, the nighttime mode will be validated in the future.
- (v) Because GLI channels are not exactly matched by MAS channels, the thresholds for each test should be further adjusted to fit the GLI channels.

This work has been completed based on existing approaches. However, there are several remaining issues that need to be investigated before and after the launch of ADEOS-II. Some tests in this algorithm should be further validated with upcoming satellite observations and/or higher resolution aircraft data. Our validation relies heavily on the use of observational data, primarily the MAS data. MODIS data will also be considered for validation when such data become available. Since the spectral distribution of the GLI and the MODIS channels are quite similar, we expect MODIS data to be very useful for testing existing approaches to the cloudy/clear discriminator and snow/sea-ice discriminator and for developing new ones as deemed necessary.

#### (6) Publications and Papers

Li, W., X. Xiong, K. Stamnes, and B. Chen, An algorithm for mapping snow/ice cover in the Arctic ocean using MODIS Airborne Simulator (MAS) data, 49th Arctic Science Conference, Alaska, October 25-28, 1998. (in press).

## D. References

- Ackerman S., K. Strabala, P. Menzel, R. Frey, C. Moeller, L. Gumley, B. Baum, C. Schaaf, and G. Riggs, 1997: Discriminating clear-sky from cloud with MODIS algorithm theoretical basis document (MOD35).
- Bunting, J.T. and R.P. d'Entremont, 1982: Improved cloud detection utilizing defense meteorological satellite program near infrared measurements. Air Force Geophysics Laboratory, Hanscom AFB, MA, AFGL-TR-82-0027, Environmental Research Papers, No. 765, 91pp.
- Curry J.A., W.B. Rossow, D. Randall, and J.L. Schramm, 1996: Overview of Arctic cloud and radiation characteristics. *J. of Climate*, 9, 1731–1764.
- Gao, B.-C., A.F.H. Goetz, and W.J. Wiscombe, 1993: Cirrus cloud detection from airborne imaging spectrometer data using the 1.38 micron water vapor band. *Geophys. Res. Lett.*, 20, 301–304.
- Gesell, G., 1989: An algorithm for snow and ice detection using AVHRR data: An extension to the APOLLO software package. *Int. J. Remote Sens.*, 10, 897–905.
- Hall, D.K., G.A. Riggs, and V.V. Salomonson, 1995: Development of methods for mapping global snow cover using Moderate Resolution Imaging Spectroradiometer data. *Remote Sens. Env.*, 54, 127–140.
- Hall, D.K., G.A. Riggs, and V.V. Salomonson, 1996: Algorithm Theoretical Basis Document (ATBD) for the MODIS snow-, Lake Ice- and Sea Ice-Mapping Algorithms.
- Jin, Z., K. Stamnes, W.F. Weeks, and S.C. Tsay, 1994: The effect of sea ice on the solar energy budget in the atmosphere-sea ice-ocean system: A model study. *J. Geophys. Res.*, 99, 25281–25294.
- Kriebel, K.T. and R.W. Saunders, 1988: An improved method for detecting clear sky and cloudy radiances from AVHRR data. *Int. J. Remote Sens.*, 9, 123–150.
- Kriebel, K.T., R.W. Saunders, and G. Gesell, 1989: Optical properties of clouds derived from fully clouds pixels. *Contr. Phys. Atmos.*, 62, 165–171.
- Kyle, H.L., R.J. Curran, W.L. Barnes, and D. Escoe, 1978: A cloud physics radiometer. Third Conference on Atmospheric Radiation, Davis, CA, 107–109.
- Nolin, A., J. Dozier, and L.A.K. Mertes, 1993: Mapping alpine snow using a spectral mixture modeling technique. *Ann. Glaciol.*, 17, 121–124.
- Rosenthal, C.W., 1993: Mapping montane snow cover at subpixel resolution from the Landsat thematic mapper. M.A. Thesis, Department of Geophysics, University of California at Santa Barbara, 70pp.
- Rossow, W.B., 1989: Measuring cloud properties from space: A review. *J. Climate*, 2, 201–213.
- Rossow, W.B. and L.C. Garder, 1993: Cloud detection using satellite measurements of infrared and visible radiances for ISCCP. *J. Climate*, 6, 2341–2369.

- Singer, F.S. and R.W. Popham, 1963: Non-meteorological observations from weather satellites, *Astronautics and Aerospace Engineering*, 1 (3), 89–92.
- Soden, B.J. and F.P. Bretherton, 1993: Upper tropospheric relative humidity from the GOES 6.7  $\mu\text{m}$  channel: Method and climatology for July 1987. *J. Geophys. Res.*, 98, 16,669–16,688.
- Stowe, L.L., S.K. Vemury, and A.V. Rao, 1994: AVHRR clear sky radiation data sets at NOAA/NESDIS. *Adv. Space Res.*, 14, 113–116.
- Wu, X., J.J. Bates, and S. Singh Khalsa, 1993: A climatology of the water vapor band brightness temperature for NOAA operational satellite. *J. Climate*, 7, 1282–1300.
- Yamanouchi, T., K. Suzuki, and S. Kawaguci, 1987 : Detection of clouds in Antarctica from infrared multispectral data of AVHRR. *J. Meteor. Soc. Japan*, 65, 949–962.